

# Experimental characterization of impact ionization coefficients for electrons and holes in GaN grown on bulk GaN substrates

Lina Cao, Jingshan Wang, Galen Harden, Hansheng Ye, Roy Stillwell, Anthony J. Hoffman, and Patrick Fay

Citation: *Appl. Phys. Lett.* **112**, 262103 (2018); doi: 10.1063/1.5031785

View online: <https://doi.org/10.1063/1.5031785>

View Table of Contents: <http://aip.scitation.org/toc/apl/112/26>

Published by the American Institute of Physics

---

## Articles you may be interested in

[Alloy disorder limited mobility of InGaN two-dimensional electron gas](#)

Applied Physics Letters **112**, 262101 (2018); 10.1063/1.5030992

[Prediction of multiband luminescence due to the gallium vacancy–oxygen defect complex in GaN](#)

Applied Physics Letters **112**, 262104 (2018); 10.1063/1.5026751

[Band alignment of AlN/ \$\beta\$ -Ga<sub>2</sub>O<sub>3</sub> heterojunction interface measured by x-ray photoelectron spectroscopy](#)

Applied Physics Letters **112**, 261602 (2018); 10.1063/1.5035372

[Leakage mechanisms in GaN-on-GaN vertical pn diodes](#)

Applied Physics Letters **112**, 233501 (2018); 10.1063/1.5033436

[Franz-Keldysh effect in GaN p-n junction diode under high reverse bias voltage](#)

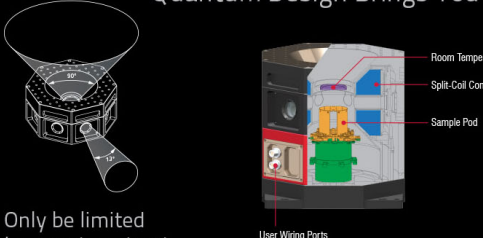
Applied Physics Letters **112**, 252104 (2018); 10.1063/1.5031215

[Negative differential resistance in GaN homojunction tunnel diodes and low voltage loss tunnel contacts](#)

Applied Physics Letters **112**, 252103 (2018); 10.1063/1.5035293

---

Quantum Design Brings You the Next Generation Magneto-Optic Cryostat




Only be limited by your imagination...

Learn More

Quantum Design  
qdusa.com/opticool5

8 Optical Access Ports: 7 Side; 1 Top  
Temperature Range: 1.7 K to 350 K  
7 T Split-Coil Conical Magnet  
Low Vibration: <10 nm peak-to-peak  
89 mm x 84 mm Sample Volume  
Automated Temperature & Magnet Control  
Cryogen Free



# Experimental characterization of impact ionization coefficients for electrons and holes in GaN grown on bulk GaN substrates

Lina Cao, Jingshan Wang, Galen Harden, Hansheng Ye, Roy Stillwell, Anthony J. Hoffman, and Patrick Fay<sup>a)</sup>

Department of Electrical Engineering, University of Notre Dame, Notre Dame, Indiana 46556, USA

(Received 30 March 2018; accepted 8 June 2018; published online 25 June 2018)

Epitaxial p-i-n structures grown on native GaN substrates have been fabricated and used to extract the impact ionization coefficients in GaN. The photomultiplication method has been used to experimentally determine the impact ionization coefficients; avalanche dominated breakdown is confirmed by variable-temperature breakdown measurements. To facilitate photomultiplication measurements of both electrons and holes, the structures include a thin pseudomorphic  $\text{In}_{0.07}\text{Ga}_{0.93}\text{N}$  layer on the cathode side of the drift layer. Illumination with 193 nm and 390 nm UV light has been performed on diodes with different intrinsic layer thicknesses. From the measured multiplication characteristics, the impact ionization coefficients of electrons ( $\alpha$ ) and holes ( $\beta$ ) were determined for GaN over the electric field range from 2 MV/cm to 3.7 MV/cm. The results show that for transport along the c-axis, holes dominate the impact ionization process at lower electric field strengths; the impact ionization coefficient of electrons becomes comparable to that of holes ( $\beta/\alpha < 5$ ) for electric field strengths above 3.3 MV/cm. © 2018 Author(s). All article content, except where otherwise noted, is licensed under a Creative Commons Attribution (CC BY) license (<http://creativecommons.org/licenses/by/4.0/>). <https://doi.org/10.1063/1.5031785>

GaN is a promising material for power electronics applications due to its wide band gap and high critical electric field.<sup>1</sup> The critical electric field is related to the onset of avalanche breakdown due to impact ionization, which puts an upper limit on the reverse blocking voltage for devices. In addition, impact ionization can be used for achieving gain in avalanche photodiodes (APDs) and impact ionization avalanche transit-time diodes (IMPATTs). However, the measurement of the impact ionization rates in GaN is challenging due to material defects such as threading dislocations from growth on foreign substrates, as well as challenges in achieving sufficient device edge termination,<sup>2,3</sup> both of which lead to early breakdown of the devices and complicate the analysis. Recent device results from GaN grown homoepitaxially on bulk GaN substrates have shown diode performance approaching material limits.<sup>4–6</sup> In addition, GaN APDs have been reported on both foreign substrates (e.g., sapphire,<sup>7</sup> SiC,<sup>8</sup> AlN<sup>9,10</sup>) and bulk GaN.<sup>11–16</sup> Despite these promising applications, detailed data on avalanche breakdown in low defect density GaN is limited; previous studies have been limited to simulations or devices on non-native substrates with large dislocation densities. In these prior reports, Oguzman *et al.*<sup>17</sup> estimated GaN's ionization rates using Monte Carlo simulations, while Kunihiro *et al.*<sup>18</sup> evaluated the electron impact ionization coefficient by investigating AlGaIn/GaN HJFETs grown on a sapphire substrate. The method used in Ref. 18 is an indirect method based on fitting parameters and only the electron ionization rate could be obtained. More recently, McClintock *et al.*<sup>19</sup> fabricated GaN p-i-n avalanche photodiodes grown on AlN templates and extracted electron and hole ionization coefficients. However, the reported electron ionization coefficients differ markedly

from both the simulation<sup>17</sup> and previous-reported measurements,<sup>18</sup> possibly due to the effects of material defects arising from the growth on dissimilar substrates.

In this letter, we present the fabrication and characterization of p-n junctions grown on single crystal bulk GaN substrates, and extract the impact ionization coefficients for both electrons and holes using the photomultiplication method.<sup>20</sup> This allows direct extraction of the native impact ionization parameters of GaN, without complications from defects.

A schematic cross section of the fabricated diodes is shown in Fig. 1(a). A ring-shaped top anode contact was used to facilitate optical coupling for the photomultiplication measurements. The structures were grown on 2-in. bulk GaN substrates by metal-organic chemical vapor deposition (MOCVD). The epitaxial layer structures (from bottom to top) consisted of 2  $\mu\text{m}$  of  $\text{n}^+\text{-GaN}$  (Si:  $4 \times 10^{18} \text{ cm}^{-3}$ ), followed by an 80 nm undoped  $\text{In}_{0.07}\text{Ga}_{0.93}\text{N}$  layer, a 150 nm or 300 nm  $\text{n-GaN}$  drift layer (Si:  $2.2\text{--}2.3 \times 10^{16} \text{ cm}^{-3}$  as measured using C-V profiling), and a 100 nm  $\text{p-GaN}$  layer (Mg:  $2 \times 10^{19} \text{ cm}^{-3}$ ). Finally, a 10 nm heavily doped  $\text{p}^{++}$  contact layer was grown to facilitate low-resistance ohmic contacts. Figure 1(b) shows the cross-sectional transmission electron microscopy (TEM) image of a fabricated device with 300 nm drift layer; except for contrast from the pseudomorphic buried InGaIn layer, the structure is uniform without obvious crystal defects. In addition, a defect density of  $3.8\text{--}4.6 \times 10^6 \text{ cm}^{-2}$  was estimated from atomic force microscopy (AFM) surface scans using the etch pit density method.<sup>21</sup> The fabrication process started with a 15 min 850 °C anneal in  $\text{N}_2$  to activate the Mg in the  $\text{p-GaN}$  layer. The top p-contact was formed by Ni (10 nm)/Au (50 nm) followed by a 10 min 500 °C thermal anneal in air to reduce contact resistance. A range of device sizes was made; the smallest had a

<sup>a)</sup>Electronic mail: pfay@nd.edu

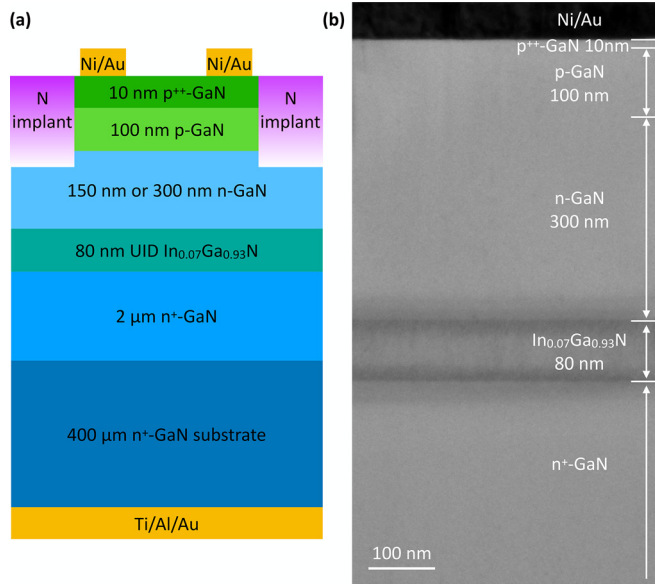


FIG. 1. (a) Schematic of the device structure and (b) cross-sectional TEM of a fabricated device with 300 nm drift layer.

ring inner diameter of 30 μm, while the largest was 200 μm. The ring width is 15 μm for all devices. A nitrogen ion implantation with an energy of 80 keV and a dose of  $1.3 \times 10^{13} \text{ cm}^{-2}$  was performed to create the edge termination. This resulted in an implant depth of 140 nm, and a defect density of  $2 \times 10^{20} \text{ cm}^{-3}$  as estimated from SRIM calculations.<sup>22</sup> By using an implanted edge termination, defect-related premature breakdown associated with mesa etch processing is avoided. Finally, a large-area Ti (50 nm)/Al (200 nm)/Au (50 nm) n-contact was deposited on the backside of the GaN substrates.

The reverse-bias dark IV characteristics of devices with 150 nm and 300 nm drift layers as a function of diameter at room temperature are shown in Figs. 2(a) and 2(b). As can be seen, the reverse current density and breakdown voltage (defined to be the voltage corresponding to a reverse current density of 1 A/cm<sup>2</sup>) are consistent across multiple devices and are independent of device area. For the 150 nm drift layer devices, the breakdown voltage is around 86 V, while that of the 300 nm devices is around 114 V. The reverse leakage current density of these devices (below breakdown) is found to be larger than for devices fabricated on nominally identical GaN p-n junctions that do not include an InGaN hole injection layer (not shown) or GaN p-i-n APDs grown on bulk GaN substrates.<sup>16</sup> The elevated leakage may be related to the InGaN layer, but the exact mechanism is not fully clear. It is possible that point defects that cannot be seen by TEM are playing a role. Figures 2(c) and 2(d) show representative temperature-dependent reverse-bias characteristics for devices with 150 nm and 300 nm thick drift layers. As can be seen, the breakdown voltage increases with increasing temperature, consistent with avalanche breakdown. The temperature dependence of the breakdown voltage is described by  $BV(T) = BV_{298K}(1 + a\Delta T)$ , where  $a$  is the temperature coefficient.<sup>23</sup> For the 150 nm drift layer devices, the temperature coefficient is  $1.46 \times 10^{-4} \text{ K}^{-1}$ ; for the 300 nm drift layer devices, the temperature coefficient is  $1.69 \times 10^{-4} \text{ K}^{-1}$ . These similar, positive temperature

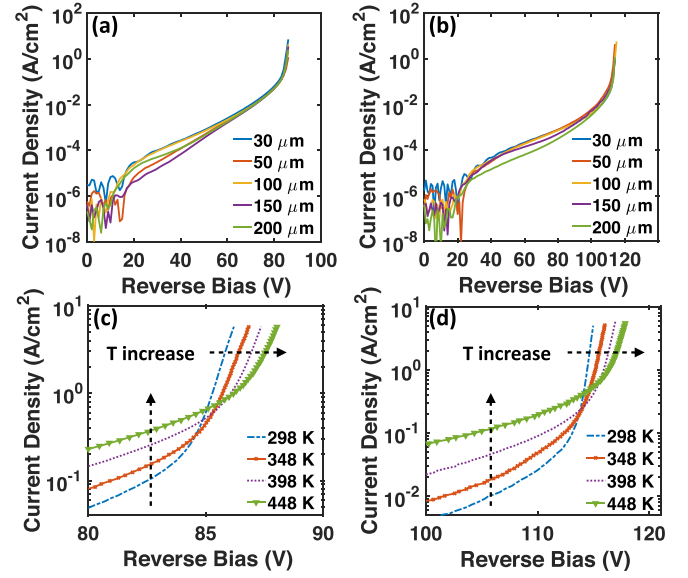


FIG. 2. Reverse-bias dark IV characteristics of different devices at room temperature as a function of device diameter with (a) 150 nm drift layer and (b) 300 nm drift layer; Temperature-dependent reverse-bias IV characteristics for typical devices with (c) 150 nm and (d) 300 nm drift layers.

coefficients indicate that the breakdown in the diodes is avalanche breakdown caused by impact ionization. This trend was observed for multiple devices over the full range of diameters (30–200 μm), indicating that edge effects do not compromise the breakdown characteristics.

Electron and hole impact ionization rates were measured using the photomultiplication method.<sup>20</sup> In this method, the p-n junction is reverse biased and photons are used to generate carriers to initiate the ionization process. When a pure electron or hole current is used to initiate the impact ionization process, it can be shown that<sup>24</sup>

$$1 - \frac{1}{M_n} = \int_0^W \alpha \exp \left[ - \int_0^x (\alpha - \beta) dx' \right] dx, \quad (1)$$

$$1 - \frac{1}{M_p} = \int_0^W \beta \exp \left[ \int_x^W (\alpha - \beta) dx' \right] dx,$$

where  $M_n$  and  $M_p$  are the electron and hole multiplication factors, and  $\alpha$  and  $\beta$  are the electron and hole impact ionization coefficients, respectively, and  $W$  is the depletion width of the p-n junction. The ionization rates  $\alpha$  and  $\beta$  are defined as the number of electron-hole pairs generated by a carrier per unit distance traveled; they are functions of position and strongly dependent on the electric field.<sup>25</sup> With the measured multiplication factors and calculated field profile of the p-n junction, the impact ionization rates can be extracted. In our experiments, as illustrated in Fig. 3(a), 193 nm pulsed UV light (2 mW/cm<sup>2</sup>) from a Coherent ExciStar-XS-200-emon UV laser was used to generate electrons in the top p-GaN layer. Since the absorption coefficient of GaN at 193 nm is larger than  $2 \times 10^5 \text{ cm}^{-1}$ ,<sup>26</sup> this results in pure electron injection into the drift layer. For pure hole injection, a 390 nm UV LED (2 mW/cm<sup>2</sup>) was used to generate holes in the buried pseudomorphic In<sub>0.07</sub>Ga<sub>0.93</sub>N layer, since this wavelength is beyond the absorption edge of GaN. In this way, we can control which carrier type initiates the

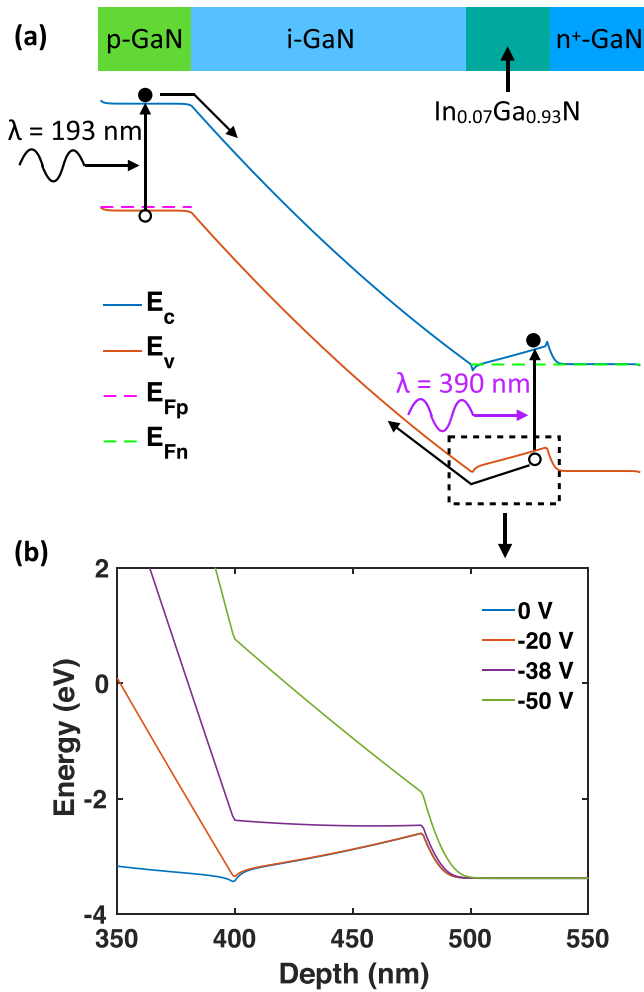


FIG. 3. (a) Band diagram of the device structure with 300 nm drift layer under reverse bias and (b) computed valence band profile under different reverse bias near the  $i\text{-GaN}/\text{In}_{0.07}\text{Ga}_{0.93}\text{N}$  interface showing the details of the polarization-induced barrier. The polarization-induced hole barrier is suppressed with increasing reverse bias.

multiplication process. Also, measuring the multiplication initiated by electrons and holes in the same junction allows us to obtain an exact solution of the integral equations in Eq. (1). Due to the low background doping, the electric field in the  $i\text{-GaN}$  region changes by less than 4% (as calculated by solving Poisson's equation numerically<sup>27</sup>) and thus can be treated as uniform. This approximation simplifies Eq. (1) and the impact ionization coefficients for electrons and holes can be extracted.

Representative measured reverse-bias current-voltage curves of typical devices with both 150 nm and 300 nm drift layers in the dark and under UV illumination are shown in Figs. 4(a) and 4(b). For the case of 193 nm UV illumination, the photocurrent depends only weakly on bias when the reverse bias is lower than 50 V for 150 nm devices and 80 V for 300 nm devices. In contrast, for 390 nm UV illumination the I-Vs show a “shoulder” due to the polarization-induced barrier at the  $i\text{-GaN}/\text{In}_{0.07}\text{Ga}_{0.93}\text{N}$  interface [see Fig. 3(b), which shows the valence band diagram calculated from a numerical solution of Poisson's equation for the 300 nm drift layer device structure]. As the reverse bias increases, the barrier flattens out and the photocurrent increases. When the reverse bias increases further, the multiplication process

starts and both the photocurrent and dark current increase sharply. The voltage at which the “shoulder” appears is in good quantitative agreement (within 2 V) of when the simulation predicts the polarization-induced barrier should be eliminated (i.e., flat-band conditions in the  $\text{InGaN}$ ). The “spike” in the  $M_n$  curves in Figs. 4(b) and 4(d) is also related to the polarization-induced barrier and quantum well for electrons that is formed by the  $i\text{-GaN}/\text{In}_{0.07}\text{Ga}_{0.93}\text{N}/n^+\text{-GaN}$  heterostructure. For voltages above the “spike” voltage, the  $\text{InGaN}$  polarization barrier is eliminated, and electrons from the drift layer pass through the  $\text{InGaN}$  layer unimpeded, leading to the expected impact ionization characteristics. In the vicinity of 40 V, however, the  $\text{InGaN}$  is near flat-band conditions. Under these conditions, hot electrons emerging from the drift layer encounter the flat-band  $\text{InGaN}$ , resulting in a local spike due to impact ionization in the narrower-band gap  $\text{InGaN}$ . Consequently, this feature is an artifact of the test structure used (to enable the photomultiplication method). This effect is more pronounced in the 300 nm drift layer case due to the larger kinetic energy of electrons entering the  $\text{InGaN}$  layer in these devices.

The multiplication factors ( $M_n$  for electrons from 193 nm illumination,  $M_p$  for holes from 390 nm illumination) are calculated using<sup>12</sup>

$$M = \frac{I_{\text{Ph}}(V) - I_{\text{Dark}}(V)}{I_{\text{Ph}}(\text{unity}) - I_{\text{Dark}}(\text{unity})}. \quad (2)$$

The multiplication factors for both samples are shown in Figs. 4(c) and 4(d). The extracted multiplication factors for electrons are noisier than that for holes because although the same average power density ( $2 \text{ mW}/\text{cm}^2$ ) was used in both cases, the number of photons (and thus carriers) that can contribute to impact ionization events for pure electron injection is much less than pure hole injection due to both absorption in the  $p\text{-GaN}$  anode layer as well as the reduced photon density at 193 nm vs. 390 nm. The references for unity photocurrent  $I_{\text{Ph}}(\text{unity})$  and dark current  $I_{\text{Dark}}(\text{unity})$  are chosen at an electric field of 1.85 MV/cm, below the onset of avalanche—so that the gain under this bias is approximately unity—but above the threshold for suppression of the polarization-induced hole barrier. From Figs. 4(c) and 4(d), one can see that the multiplication factors for electrons are smaller than those for holes over a wide reverse bias range, until close to breakdown for both device structures. The hole-initiated multiplication starts at an electric field of approximately 1.9 MV/cm, and significant multiplication is observed well below the breakdown voltage. In contrast, electron-initiated multiplication remains negligible ( $M_n \sim 1$ ) for a large reverse bias range, and becomes significant only very close to breakdown, around 2.8 MV/cm. This suggests that there is a strong asymmetry between electron and hole impact ionization coefficients, and holes dominate the charge multiplication process when the reverse bias is low.

From Eq. (1), one can calculate the impact ionization coefficients for electrons ( $\alpha$ ) and holes ( $\beta$ ); the results are plotted in Fig. 5. Combining the results from devices with 150 nm and 300 nm drift layers allows extraction of the impact ionization rates over a wide electric field range. A



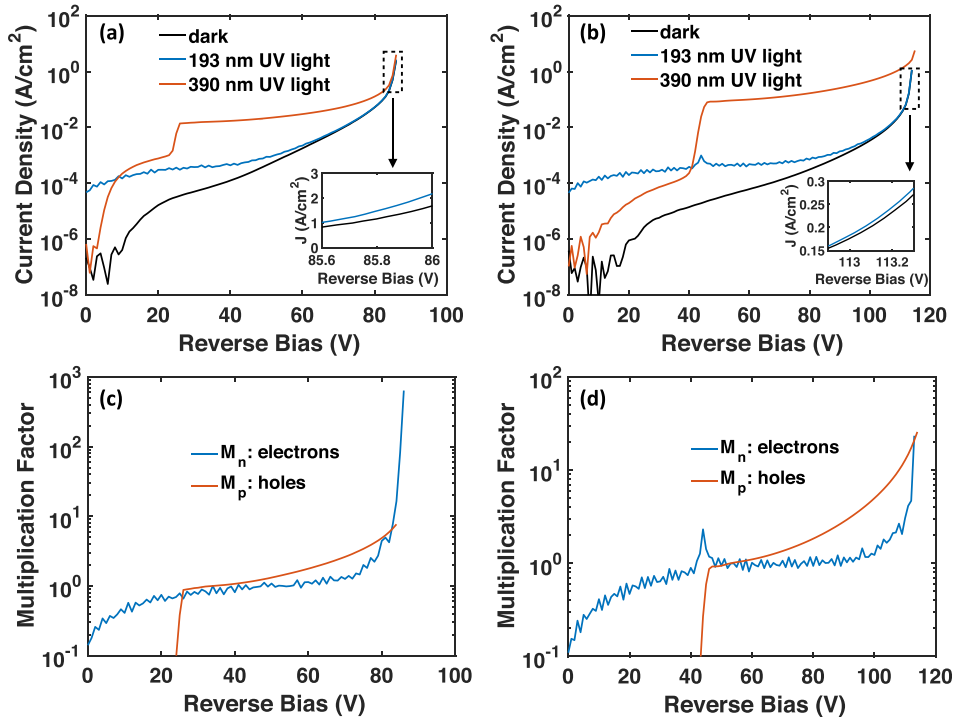


FIG. 4. Reverse IV curves of the diodes under dark and UV illumination for (a) 150 nm and (b) 300 nm drift layer devices; multiplication factors for electrons ( $M_n$ ) and holes ( $M_p$ ) for (c) 150 nm and (d) 300 nm drift layer devices.

least-squares fit to the electron and hole impact ionization rates using Chynoweth's equation<sup>28</sup> yields

$$\begin{aligned}\alpha(E) &= 4.48 \times 10^8 \exp(-3.39 \times 10^7/E), \\ \beta(E) &= 7.13 \times 10^6 \exp(-1.46 \times 10^7/E).\end{aligned}\quad (3)$$

In addition, fits were performed for a unity reference of 1.6 MV/cm, since in these devices the threshold for impact ionization is not entirely clear. The electron coefficients were found to be nearly identical, while those for holes were found to shift modestly to  $3.11 \times 10^6 \exp(-1.20 \times 10^7/E)$ . For comparison with theory, we performed a least-squares fit to the data predicted by Monte Carlo simulation;<sup>17</sup> the resulting impact ionization rates for c-axis transport are

$\alpha(E) = 5.02 \times 10^8 \exp(-3.41 \times 10^7/E)$  and  $\beta(E) = 6.80 \times 10^6 \exp(-1.87 \times 10^7/E)$ . As can be seen, the results presented here are in good general agreement with these theoretical predictions. The disagreement in the hole ionization coefficients is due mostly to a vertical offset of the curve; the field-dependent term is in good agreement with theory. The origin of this discrepancy needs further investigation.

As shown in Fig. 5, at low electric fields the hole ionization rate is much larger than the electron ionization rate. The  $\beta/\alpha$  ratio decreases from 37.5 at 2.5 MV/cm to 5.2 at 3.3 MV/cm. This observed asymmetry between electron and hole ionization coefficients is attractive for the design of low-noise GaN APDs, and suggests that to achieve low noise in GaN APDs it may be advantageous to have the avalanche process be initiated by holes.

Since the diodes reported here were grown on bulk GaN substrates with low defect densities and with an implanted edge termination that results in little contribution from the device perimeter, they provide an unfiltered view of the impact ionization process, without mixing in other physical effects related to defects or fabrication limitations. The electron ionization coefficients reported here are in good agreement with simulation<sup>17</sup> as well as Kunihiro's results on sapphire, which gives  $\alpha(E) = 2.9 \times 10^8 \exp(-3.4 \times 10^7/E)$ ,<sup>18</sup> but differs significantly from McClintock's results on AlN.<sup>19</sup> In addition, as can be seen in Fig. 5, the slopes of the measured impact ionization coefficients for electrons and holes differ by more than 2 times, consistent with theoretical predictions.<sup>17</sup> This is in contrast to the observation of very similar slopes for both electrons and holes for devices on AlN templates.<sup>19</sup>

In summary, the breakdown and avalanche multiplication characteristics of GaN p-n junction devices grown on native GaN substrates have been investigated. Electron and hole impact ionization coefficients for GaN epitaxial structures grown on bulk GaN substrates have been extracted

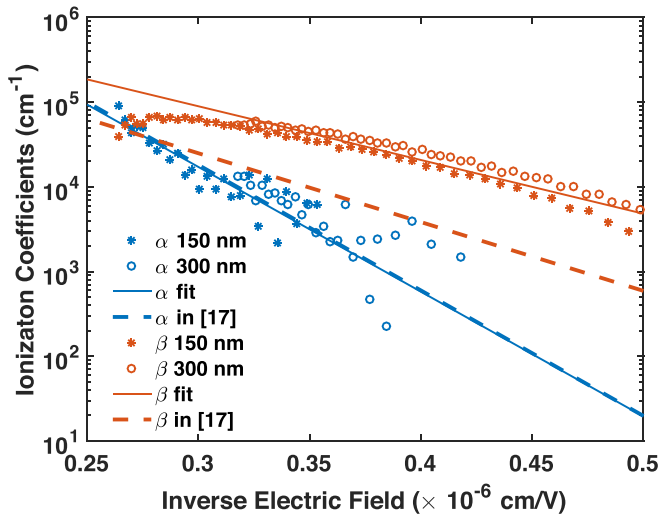


FIG. 5. Impact ionization coefficients for electrons (blue) and holes (orange). Points show the measured impact ionization rates and solid lines represent the Chynoweth equation fit to the experimental results while dashed lines represent the Chynoweth equation fit to the simulation results in Ref. 17.

using the photomultiplication method. In contrast to previous reports, the results presented here are in good general agreement with the theoretical impact ionization rates predicted using Monte Carlo simulation,<sup>17</sup> indicating that defect and edge effects have been adequately suppressed. The experimentally validated impact ionization coefficients reported here may be valuable for the design of improved optoelectronic, microwave, and power devices.

This work was supported by the U.S. Office of Naval Research, Grant No. N00014-16-1-2850, Paul Maki program manager.

- <sup>1</sup>U. K. Mishra, L. Shen, T. E. Kazior, and Y.-F. Wu, *Proc. IEEE* **96**, 287 (2008).
- <sup>2</sup>Y. Zhang, M. Sun, D. Piedra, M. Azize, X. Zhang, T. Fujishima, and T. Palacios, *IEEE Electron Device Lett.* **35**, 618 (2014).
- <sup>3</sup>X. Zou, X. Zhang, X. Lu, C. W. Tang, and K. M. Lau, *IEEE Electron Device Lett.* **37**, 636 (2016).
- <sup>4</sup>J. Wang, L. Cao, J. Xie, E. Beam, R. McCarthy, C. Youtsey, and P. Fay, in *2017 IEEE International Electron Devices Meeting (IEDM)* (IEEE, 2017), pp. 6–9.
- <sup>5</sup>M. Qi, K. Nomoto, M. Zhu, Z. Hu, Y. Zhao, V. Protasenko, B. Song, X. Yan, G. Li, J. Verma, S. Bader, P. Fay, H. G. Xing, and D. Jena, *Appl. Phys. Lett.* **107**, 232101 (2015).
- <sup>6</sup>A. M. Armstrong, B. N. Bryant, M. H. Crawford, D. D. Koleske, S. R. Lee, and J. J. Wierer, Jr., *J. Appl. Phys.* **117**, 134501 (2015).
- <sup>7</sup>J. Carrano, D. Lambert, C. Eiting, C. Collins, T. Li, S. Wang, B. Yang, A. Beck, R. Dupuis, and J. Campbell, *Appl. Phys. Lett.* **76**, 924 (2000).
- <sup>8</sup>Q. Zhou, D. C. McIntosh, Z. Lu, J. C. Campbell, A. V. Sampath, H. Shen, and M. Wraback, *Appl. Phys. Lett.* **99**, 131110 (2011).
- <sup>9</sup>K. Minder, J. Pau, R. McClintock, P. Kung, C. Bayram, M. Razeghi, and D. Silversmith, *Appl. Phys. Lett.* **91**, 073513 (2007).
- <sup>10</sup>J. Pau, C. Bayram, R. McClintock, M. Razeghi, and D. Silversmith, *Appl. Phys. Lett.* **92**, 101120 (2008).
- <sup>11</sup>J. Limb, D. Yoo, J. Ryou, W. Lee, S. Shen, R. Dupuis, M. Reed, C. Collins, M. Wraback, D. Hanser *et al.*, *Appl. Phys. Lett.* **89**, 011112 (2006).
- <sup>12</sup>S.-C. Shen, Y. Zhang, D. Yoo, J.-B. Limb, J.-H. Ryou, P. D. Yoder, and R. D. Dupuis, *IEEE Photonics Technol. Lett.* **19**, 1744 (2007).
- <sup>13</sup>S. Choi, H. J. Kim, Y. Zhang, X. Bai, D. Yoo, J. Limb, J.-H. Ryou, S.-C. Shen, P. Yoder, and R. D. Dupuis, *IEEE Photonics Technol. Lett.* **21**, 1526 (2009).
- <sup>14</sup>Y. Zhang, S.-C. Shen, H. J. Kim, S. Choi, J.-H. Ryou, R. D. Dupuis, and B. Narayan, *Appl. Phys. Lett.* **94**, 221109 (2009).
- <sup>15</sup>E. Cicek, Z. Vashaei, R. McClintock, C. Bayram, and M. Razeghi, *Appl. Phys. Lett.* **96**, 261107 (2010).
- <sup>16</sup>M.-H. Ji, J. Kim, T. Detchprohm, R. D. Dupuis, A. K. Sood, N. K. Dhar, and J. Lewis, *IEEE Photonics Technol. Lett.* **28**, 2015 (2016).
- <sup>17</sup>I. H. Oğuzman, E. Bellotti, K. F. Brennan, J. Kolnik, R. Wang, and P. P. Ruden, *J. Appl. Phys.* **81**, 7827 (1997).
- <sup>18</sup>K. Kunihiro, K. Kasahara, Y. Takahashi, and Y. Ohno, *IEEE Electron Device Lett.* **20**, 608 (1999).
- <sup>19</sup>R. McClintock, J. Pau, K. Minder, C. Bayram, P. Kung, and M. Razeghi, *Appl. Phys. Lett.* **90**, 141112 (2007).
- <sup>20</sup>R. Van Overstraeten and H. De Man, *Solid-State Electron.* **13**, 583 (1970).
- <sup>21</sup>P. Visconti, K. Jones, M. A. Reshchikov, R. Cingolani, H. Morkoç, and R. Molnar, *Appl. Phys. Lett.* **77**, 3532 (2000).
- <sup>22</sup>J. F. Ziegler, M. D. Ziegler, and J. P. Biersack, *Nucl. Instrum. Methods Phys. Res. B* **268**, 1818 (2010).
- <sup>23</sup>I. C. Kizilyalli, A. P. Edwards, O. Aktas, T. Prunty, and D. Bour, *IEEE Trans. Electron Devices* **62**, 414 (2015).
- <sup>24</sup>C. Lee, R. Logan, R. Batdorf, J. Kleimack, and W. Wiegmann, *Phys. Rev.* **134**, A761 (1964).
- <sup>25</sup>W. Maes, K. De Meyer, and R. Van Overstraeten, *Solid-State Electron.* **33**, 705 (1990).
- <sup>26</sup>J. Muth, J. Lee, I. Shmagin, R. Kolbas, H. Casey, Jr., B. Keller, U. Mishra, and S. DenBaars, *Appl. Phys. Lett.* **71**, 2572 (1997).
- <sup>27</sup>G. Snider, I.-H. Tan, and E. Hu, *J. Appl. Phys.* **68**, 2849 (1990).
- <sup>28</sup>A. G. Chynoweth, *Phys. Rev.* **109**, 1537 (1958).